Acta Technica Napocensis: Civil Engineering & Architecture
Volume 61, No. 1, (2018)
Journal homepage: http://constructii.utcluj.ro/ActaCivilEng
ISSN 1221-5848

Experimental and Numerical Modal Analysis of an Existing Hydraulic Structure

Ahmed A. Elwy[1a], Boshra A. El-taly[1]*, and Yasser A. El-Hakem[2b*]

[1]Civil Engineering Department, Faculty of Engineering, Minoufia University, Egypt.
[2]Construction Research Institute, National Water Research Center, Egypt.

(Received 15 April 2018, Accepted 29 May 2018)

Abstract. The dynamic properties of a hydraulic structure in terms of frequency/time period, mode shape and damping properties play the major role in its seismic design or assessment of existing hydraulic structures. The seismic design depends on the value of the ground acceleration which is a function in the natural period of the structure. Therefore, the problem of choosing the value of the ground acceleration in the design or assessment reflects on the cost needed for establishing or habitation of existing hydraulic structure. Also, most of the existing hydraulic structures in Egypt, such as barrages were built using bricks or plain concrete. These materials have low resistance against tension stresses due to seismic excitation. The current research aims to estimate the dynamic properties of a hydraulic structure as the first step to estimate its behavior under the seismic loads. The Old Rayah Menoufia Barrage – Egypt was selected as a case study. The dynamic properties of the barrage were investigated experimentally. The studied barrage was simulated in three-dimensional Finite Element (FE) models using ANSYS release 15 Software. The water dynamic pressure was considered in all employed FE models. The Soil-Structure Interaction (SSI) was not considered in the analysis as an Initial Model (IM) then it was considered in Updating Models (UMs) with different phases. The SSI was considered by changing the base condition from fixed to soil subgrade reactions. The horizontal subgrade reactions were considered as a percentage of the vertical reaction (0%, 10%, 30% and 50% for UM1, UM2, UM3 and UM4, respectively). The results showed that the horizontal subgrade reaction should be considered in the analysis, as neglecting it or considering it with either more or not sufficient stiffness gives misleading results.

Keywords: barrage: finite element simulation: water dynamic pressure: soil-structure interaction: experimental modal analysis.

1. Introduction

Experimental Modal Tests (EMTs) are economical and practical dynamic tests that identify accurately modal parameters of civil engineering structures. Therefore, specialists usually conduct these tests before rehabilitation works on civil engineering structures. Also, they provide experimental information that can be used for the design and dynamic monitoring and for the determination of a set of modal properties of these structures (Kortiš *et al.* 2016 and Shaheen *et al.* 2013). This technique has widely grown since the advent of the digital Fast Fourier Transform (FFT) spectrum analyzer in the early 1970's (Rahman 2009 and Payab and Ahmadifar 2015). EMA is divided into two types: forced vibration testing and ambient vibration testing. The force method is conducted by exciting the structure with a known valued force, which will induce a condition of free vibration. The ambient vibration testing is conducted under the real operating condition of the structure, which is based on vibrations that may be induced by traffic, waves, quakes, or wind as natural or environmental excitations (Brownjohn 2003, Diaferio *et al.* 2015, Comanducci *et al.* 2017 and Bajric *et al.* 2015). The first study was carried out to measure the modal parameters of an aircraft in order to predict accurately the problem of flutter (Balmes *et al.* 1995) and then they were extended to apply in various applications in civil engineering. Khalil *et al.* (1998) performed nondestructive evaluation of a three-span steel welded plate girder bridge using modal testing techniques. The bridge was constructed in

*Corresponding author, Associate Professor, E-mail: boushra_eltaly@yahoo.com
[a]Ms.C. Student, E-mail: Eng_ahmedashrafelwy@yahoo.com
[b]Professor, E-mail: yelhakem@yahoo.com

1972. It consists of 200 mm thick reinforced concrete deck slab. In the 1997, deck rehabilitation was carried out that added a 40 mm of concrete overlay to the current deck. This research applied ambient excitation to determine location and size of defects in the bridge. Pandey *et al.* (2004) studied the dynamic characteristics of a barrage at various stages of construction. They considered fourteen stages for analysis and performed the free vibration analysis at each stage. Their results showed that the underlying soil affects the behavior of the structure. Graygordóbil (2005) presented previous literature reviews of the application of the dynamic testing on ancient structures. His research pointed out three necessary components to achieve the success of a dynamic test on an ancient structure: pre-define of test's objectives, the careful organization of all test's details and the manful fashion presentation of results. Ramos *et al.* (2006) carried out damage identification in masonry structures at each damage stage. Haritos *et al.* (2013) investigated dynamic testing for the skew bridge. Eltaly *et al.* (2014) carried out an experimental modal analysis for elevated steel water tanks. The tanks were excited by applying a random impact at the base in the two horizontal directions (X&Y) alternately using the impact hammer. Calcina *et al.* (2014) performed the ambient vibration tests on an arch dam. The results showed that the radial component of the motion affected by the vibration properties of the dam. Kandil *et al.* (2016) and Saudi *et al.* (2016) applied ambient vibration test on wind turbine and simulated the turbine with FE modeling. The FE model gave good results compared with the experimental results.

The potential of considering the fluid structure interaction in the dynamic analysis is so necessary. The sloshing and the dynamic pressure of water effect on the dynamic response of a structure that is not ever neglect. There are several approaches to consider fluid–structure interaction such as simplified methods with Housner's two-mass representation (Housner 1963), multi-mass representation (Charatpangoon *et al.* 2014), added mass in a ''solid'' Finite Element Model (FEM), and provisions of the design codes (Eurocode-8, 2003, API 650, 1998 or ACI 350.3, 2001). Livaoglu and Dogangun (2006) presented the comparison between these methods. In their conclusion, they recommended to use the impulsive pressure distribution given by Housner (Housner 1963) for analysis of lock structures for determination of the added hydrodynamic mass. An important study on mechanical systems modeling for fluid–structure interaction was published by Axisa and Antunes (2007). For more complex models and an exhaustive analysis incorporating Lagrangian and Eulerian (Kuo 1982), and Lagrangian–Eulerian approaches in Finite Element Method formulations were used.

During the last 40 years, the Soil-Structure Interaction (SSI) has achieved a major interest among engineers and researchers in whole fields of structural analysis. The analysis investigations included two kinds: numerical simulation and analytical methods. Analytical methods have been popular in the 1970's since the development of computer technology. While the quick progress in the art of computer science caused a wide use of numerical simulation methods in studying the SSI (Li *et al.* 2004). Raychowdhury and Singh (2012) studied the effective of nonlinearity SSI in the analysis of low rise steel moment-resisting frames subjected to earthquake load. Their results showed that the story displacement demand increasing by considering nonlinear SSI. Swapnal (2015) studied the effect of SSI on the behavior of gravity dam due to seismic forces using FE analysis software ANSYS version 14. They have modeled the relevant amount of soil bottom and around of the gravity dam for real simulation of the in-situ conditions. His results indicated that the displacement was noticed to be higher in the case of considering the SSI in the analysis than the fixed base. Varughese and Nikithan (2016) determined the seismic behavior of concrete gravity dams using ANSYS Version 15. They modeled the dam and the beneath foundation with 2D plane strain element (Plane42) and the reservoir with fluid acoustic element (Fluid29) of some consideration of fluid-structure interaction. In their model, both of flow pressure and structure deflection were taking into consideration. They took into consideration fixed condition for dam base. Valeti *et al.* (2016) considered a simplified model to determine the behavior of an elevated aqueduct under seismic load. They considered different base conditions: fixed base, nonlinear base conditions and elastic-base (subgrade reactions). Housner's

model was used to simulate water contained aqueduct channels. Farghaly in 2017 employed 2-D models to simulate two adjacent buildings with 6 and 12 floors and with considering SSI. Soil was simulated by 2D shell elements in contact with the foundations.

Most of the hydraulic structures in Egypt are designed based on static load approach without consideration of vibration on the structure during the design stage. The vibration design is mostly taken into consideration in the high-rise building design only. However, Egypt is not located in the earthquake and typhoon zone, but the incidents that happened lately such as the 1992 earthquake had a huge impact on most structures of Egypt. Therefore, this work looks forward in the determination of the dynamic properties, including natural frequencies, mode shapes, damping values of The Old Rayah Menoufi Barrage – Egypt from ambient vibration testing. An Initial Model (IM) was adopted to control the Experimental Work (EW). In IM all structural elements of the barrage were simulated using solid65 with its corresponding material properties. The water through the vents and the lock chamber of the barrage was modeled using simplified mass simulation. The fixed base condition of the barrage was adopted in this model, neglecting the SSI. Great significant differences were observed between the EW and IM, so four Updated Models (UM1, 2, 3, and 4) were mounted to decrease this variation and achieve more realistic results close to the EW. In the updated models, the SSI was considered by changing the base condition from fixed to soil subgrade reactions. The vertical stiffness of the subgrade reactions was chosen as an average value of the Bowles` subgrade reactions (Bowles (1988)), according to the soil properties under the base of the used barrage. The horizontal subgrade reactions were considered as a percentage of the vertical reaction (0%, 10%, 30% and 50% for UM1, UM2, UM3 and UM4, respectively). This ratio was missing in references and there is not any guide to control it. Even though, the recent studies that were conducted on the estimation of horizontal subgrade reaction were mainly for the pile studies. The updated models are compared with the EW to obtain the most realistic results. These comparisons showed that UM3 with the ratio of 30% of the vertical subgrade reaction is the most matching model that is close to the EW.

2. Old Rayah Menoufia barrage

The Old Rayah Menoufia Barrage is one of the oldest existing hydraulic structures in Egypt that was permitted to be tested by the Construction Research Institute (CRI) - National Water Research Centre (NWRC) - Egypt. Construction of this structure was completed in August 1910. This barrage consists of eight concrete piers and a lock wall. Each pier supports a concrete arch that carries the barrage road. At the end of the barrage, a steel bridge located over the lock with an ability of being lifted to permit the navigation through the lock. Supporting piers, abutments, and wing walls were built over two level rafts of varied in material founded on the canal bed. The down/up-streams are represented in Fig. 1. Also, the general dimensions and the hydraulic data of the barrage are summarized in Table 1 and Table 2, respectively.

The material properties of the barrage elements are illustrated in Table 3. It was assumed to be considered as the material properties of Zefta barrage - Egypt, which is quite similar to this studied barrage in material, in dimension, and in construction age. These properties were previously determined in several technical reports that were conducted on the Zefta barrage (Sogreah 2005, Ace 1996 and Lahmeyer 2004).

(a) Downstream (b) Upstream

Fig.1 The downstream and upstream of the barrage

Table 1 General dimensions of the Old Rayah Menoufi barrage

Item		Dimension or levels
Total number of gate openings		9.00
Gate opening		5.00 m
Pier height		7.50 m
Roadway (level)		(20.44) m
Top of parapets (level)		(21.40) m
Roadway width including sidewalks		10.00 m
Pier	Length	15.50 m
	Thickness	2.00 m
	Top elevation (level)	(18.00) m
	Bottom elevation (level)	(10.50) m
Lock pier	Length	79.0 m
	Maximum thickness	6.70 m
	Minimum thickness	4.00 m
	Top elevation (level)	(19.30) m
	Bottom elevation (level)	(10.50) m
Concrete apron	Length (regulator)	60.00 m
	Maximum thickness	3.00 m
	Minimum thickness	3.00 m

Table 2 Hydraulic data of the selected barrage

Item	Maximum upstream water level	Downstream water level
Level	(16.60) m	(16.60) m

Table 3 Material properties of the barrage

Element	Type	Density (ρ) kg	Modulus of elasticity (E) GPa	Poisson's ratio (μ)
Raft at F.L (7.50) m	Cement concrete 4:1	2200	11	0.35
Raft at F.L (8.50) m	Rubble in cement mortar 4:1	2240	36	0.35
Arches	Cement concrete 4:1	2200	18	0.35
Piers and lock wall	Masonry	2230	31	0.30
Abutments	Masonry	2230	31	0.30
Steps	Masonry	1690	3.4	0.30
Parapet	Masonry	1690	3.4	0.30
Road	Asphalt	1800	-	-

3. Experimental modal testing

The response of the structure under testing was determined by a set of sensors, located at different measurement points over one intermediate vent. The number of these points was chosen in order to

achieve the spatial resolution needed for appropriately determining the shape of the most relevant mode shapes of vibration (according to preliminary finite element modelling). In traditional measuring chains, the continuous electrical signal produced by each sensor is transmitted by electrical cables to a data acquisition system (Mohamed 2015). A digital card controls the measuring process and converts analogue signals to digital ones. Then, adopted cards transmit the digital data to a laptop computer for the purpose of data storing and analysing. These adopted instruments are represented in Fig. 2.

An ambient vibration test was applied on Old Rayah Menoufia Barrage. It was based on the use of accelerometers to record barrage acceleration response due to excitation by heavy truck. With the purpose of identifying, most possible vibration modes, essentially of transversal and vertical bending nature were recorded. There were just two days available for this test: one was to prepare the test and the other was the test day. The measurement location grid was attached to the barrage longitudinal axis as shown in Fig. 3. A test was carried out over one intermediate vent (see Fig. 4), as barrage consists of replicated vents that are same in whole geometry, fill, and material properties. This tested vent will indicate for the whole barrage's behavior. Twelve accelerometers are mounted on the tested vent so as to capture symmetric and anti-symmetric vertical bending modes, torsion modes, and the horizontal deformations.

Channels from 1 to 6 are vertical sensors and channels 7 to 12 are horizontal sensors to capture the vertical and horizontal deformations. The recorders were controlled to capture with a sampling rate of 500 Hz. The test took three hours, including test preprocessing. So, it is noticeable to realize that, with the adopted equipment, test took less than one day for performing the required measurements. Three records were selected to achieve and acceptable accuracy. The data collected during these free vibration tests were filtered and fundamental modal parameters were determined, corresponding mode shapes were obtained as well.

The passage of the truck over the artificial obstacle allows the barrage to be excited in the vertical direction. The first mode shape of the barrage from the finite element analysis has a lateral deformation. Therefore, there was a need to apply a new technique of excitation to develop a lateral and vertical deformation/response of the barrage together. This technique was based on letting the truck move over the obstacle with average speed to 60 km/h (vertical excitation), then instantly stopping the truck to apply braking force on the barrage. This braking force is responsible for allowing the lateral excitation of the barrage. This technique has been developed the required lateral and vertical mode shape that will be shown in the following sections.

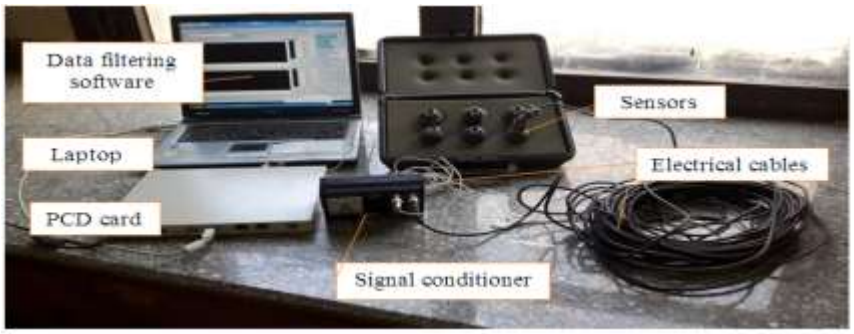

Fig. 2 The adopted instruments

After the excitation of the barrage, data were collected for each channel as signal records in the sample of acceleration-time response record, as shown in Fig. 5. Due to the lack of sensors, and instruments, the response of the barrage was recorded for the interior vent only. It is supposed to indicate the whole behavior of the barrage. Therefore, the response of the far structural elements that is away from the interior vent is not captured. The collected data were processed and filtered for each channel with filter options: bandwidth pass filter, lower frequency with a value of 0 Hz, upper frequency with a value of 40 Hz, and filter order equals to 6.

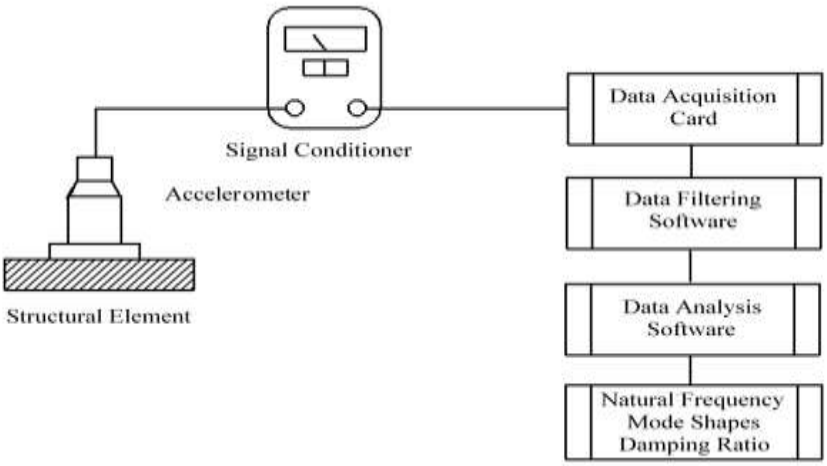

Fig. 3 The proceedings of data acquisition

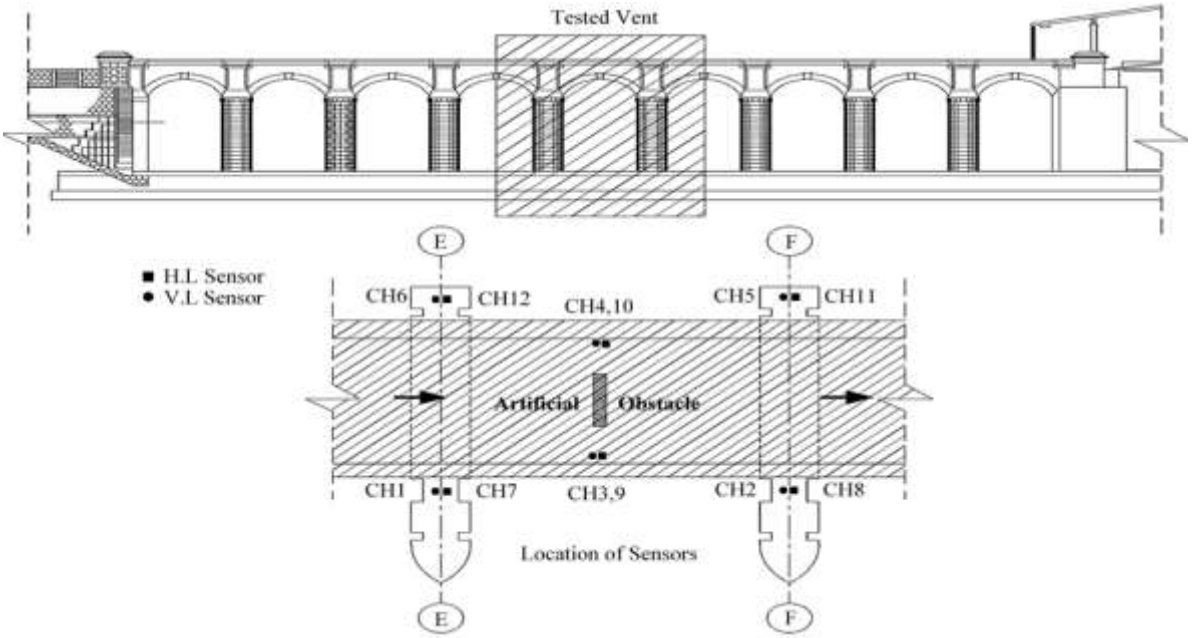

Fig. 4 Location of sensors over the intermediate tested vent

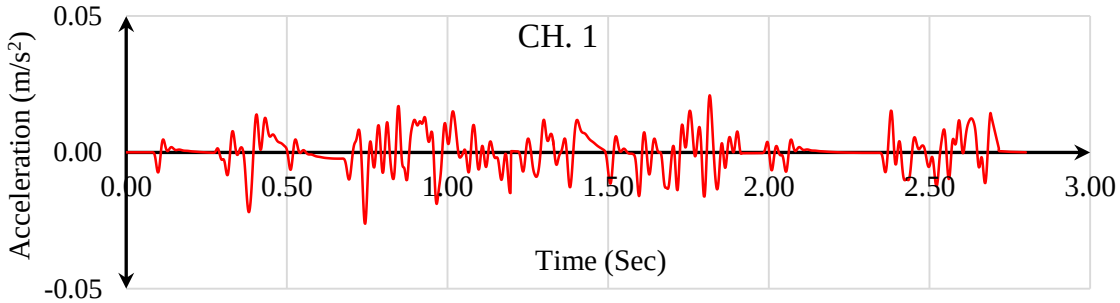

Fig. 5 Examples of recorded signal

To estimate the vibration properties of the barrage, the collected data subjected to curve fitting processes after the Fast Fourier Transformation (FFT). FFT transforms the data from acceleration-time domain to acceleration-frequency domain, as represented in Fig. 6 (for channel 1). While, the curve fitting processes involve three stages: counting mode shapes, determining the frequency and damping properties, and estimating the residues and save the mode shapes. Some of the obtained mode shapes after filtering the records and curve fitting are concluded as represented in Table 4.

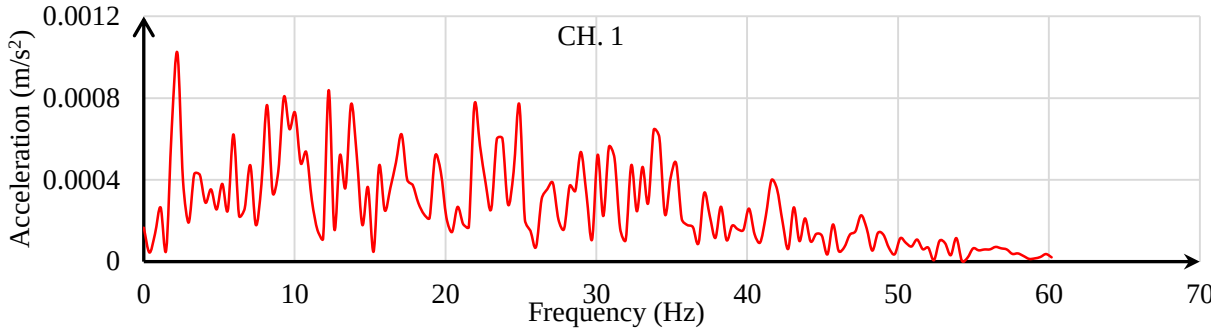

Fig. 6 FFT transformation of the signal records for channel 1

Table 4 The frequency value of captured mode shape from the Experimental Work (EW)

Mode Shape	1st	2nd	3rd	4th	5th	6th	7th	8th
Frequency (Hz)	7.96	13.2	16.8	17.0	18.6	20.1	20.8	26.9
Damping (%)	0.837	0.535	0.35	0.589	1.54	0.00343	0.198	0.197

4. Finite element modeling

In the linear modal analysis, Block Lanczos solver performance output was used to extract mode shapes and natural frequencies. The Block Lanczos method uses an assembled stiffness and mass matrix in addition to factoring matrices that are a combination of the mass and stiffness matrices computed at various shift points (ANSYS 2013). The numerical analysis gives many natural frequencies and their corresponding mode shapes. The FE model produced about 100 modes of shapes in the frequency ranges between 0.1 and 1000 Hz. These mode shapes consist of local and global ones.

4.1 Used elements

Solid65 element is used for simulating the concrete or the mortar with and without reinforcements. The element has one solid material and up to three rebar materials in the three directions. The solid material is used to model the concrete. The rebar capability is used for modeling reinforcement behavior. Reinforcement is specified by its material, volume ratio and orientation angles. The volume ratio is defined as the rebar volume divided by the total element volume. The orientation is defined by two angles in degrees (θ and φ) from the element coordinate system as shown in Fig. 7 (Eltaly *et al.* 2017). This element has crushing and cracking capabilities. The most important aspect of this element is the treatment of nonlinear material properties. The concrete and mortar are capable of cracking (in the three orthogonal directions), crushing, plastic deformation and creep. The rebar (reinforcement) are capable of tension and compression, but not shear. The rebar is also capable of plastic deformation and creep (ANSYS 2013). The weight of the Asphalt and water is represented by a Mass21 element (Kandil *et al.* 2016 and Saudi *et al.* 2016). This element is a point element having up to six degrees of freedom: translations in the x, y, and z directions and rotations about the nodal x, y, and z axes.

Combine14 element has either longitudinal or torsional capability which could be adopted in 1-D, 2-D, or 3-D applications. The torsional option is a rotational element that got three degrees of freedom at each node: x, y, and z axes rotations, without any axial loads or bending consideration. The longitudinal option is a purely uniaxial tension-compression element without considering of bending or torsion. Its degrees of freedom are up to three at each node: translations in x, y, and z directions. This element has no mass. Damping or spring capabilities may be eliminated from the element options by setting K or C_V equal to zero, respectively. The element is defined through two nodes (i, j). The geometry, node locations and the coordinate system for this element are shown in Fig. 8. This element could be used in either linear or non-linear solution (ANSYS 2013).

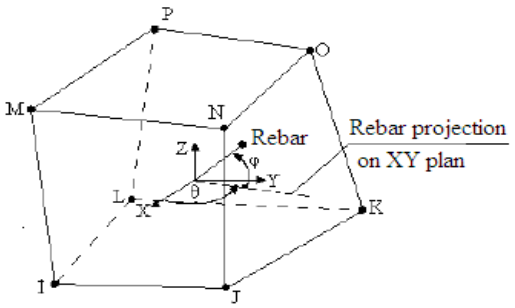

Fig. 7 Solid65 element (ANSYS 2013 and ELtaly *et al.* 2017)

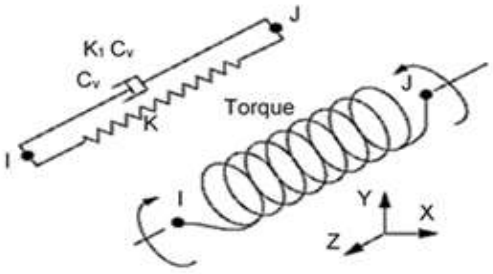

Fig. 8 Combine14 Element (ANSYS 2013)

4.2 Fluid–structure interaction

Housner (1963) carried out his study on liquid tank proposed to horizontal ground accelerations. The contained liquid was simulated by two masses: impulsive and convective mass, as shown in Fig. 9. He assumed that the tank walls are rigid, the liquid is incompressible, the liquid displacements are small, the tank is open tank and the tank is with vertical side walls and horizontal bottom that is symmetrical with respect to the vertical X-Y and Z –Y planes in order to derived equations for estimating the values and the height of the two masses (Eq. (1) to Eq. (6)). These equations are functions in the tank dimensions and the liquid elevations.

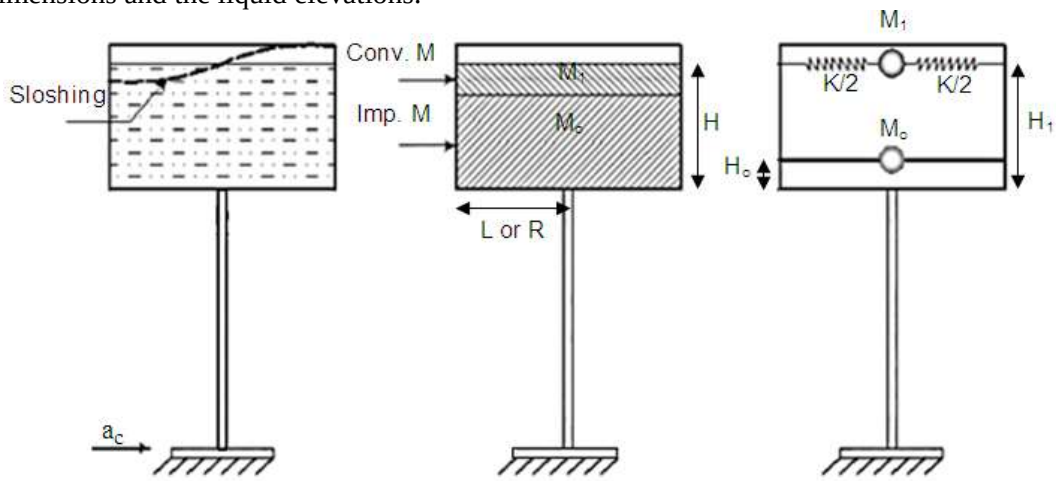

Fig. 9 Housner simulation of containing liquid (Housner 1963)

$$M_o = \frac{\tanh(1.7\ L/H)}{1.7\ L/H}\ M \tag{1}$$

$$M_1 = \frac{0.83\tanh(1.6\ H/L)}{1.8\ H/L}\ M \tag{2}$$

$$H_o = 0.38\left[1+\propto\left(\frac{M_1}{M}\left(\frac{L}{H}\right)^2 - 1\right)\right]H \tag{3}$$

$$H_1 = \left[1 - 0.333\frac{M_1}{M}\left(\frac{L}{H}\right)^2 + 0.63\,\beta\times\frac{L}{H}\sqrt{0.28\left(\frac{M\,L}{M_1 H}\right)^2 - 1}\right]H \tag{4}$$

$$K_1 = 3\ g\ \frac{{M_1}^2}{M}\times\frac{H}{L^2} \tag{5}$$

$$T_w = 2\,\pi\sqrt{\frac{M_1}{M}} \tag{6}$$

Where: M is the mass of the contained liquid, H is the depth at rest of the contained liquid, L is the half length of rectangular tank, M_o is the impulsive mass, M_1 is the convective mass, K_1 is the spring stiffness, H_o and H_1 are the height of M_o and M_1 respectively, T_w is the period of vibration and g is the gravity acceleration and α=1.33, β=2.0.

4.3 Initial model (IM)

In this model, Solid65 elements (ANSYS 2013) were adopted to model the whole barrage structural members (such as foundations, piers, walls, etc.) as shown in Fig. 10. Mass21 used to simulate added masses on the barrages that were induced from dynamics of water or dead loads on structures. Masses of dead loads were added as 45 Kg for asphalt own weight, 829 kg for parapet own weight with height of 2.00 m and 1794 kg for parapet own weight with height of 4.40 m. These masses were assigned on the nodes attached to the location of applied surface and they were defined in the three dimensional with the same value. The barrage model contains whole structural members with corresponding real dimension of the barrage. The material properties were defined as isotropic and homogenous properties. The size of mesh was 0.5 m x 0.5 m and the sweep tool was used to apply meshing for whole structure. The fixed base boundary condition was adopted in this model.

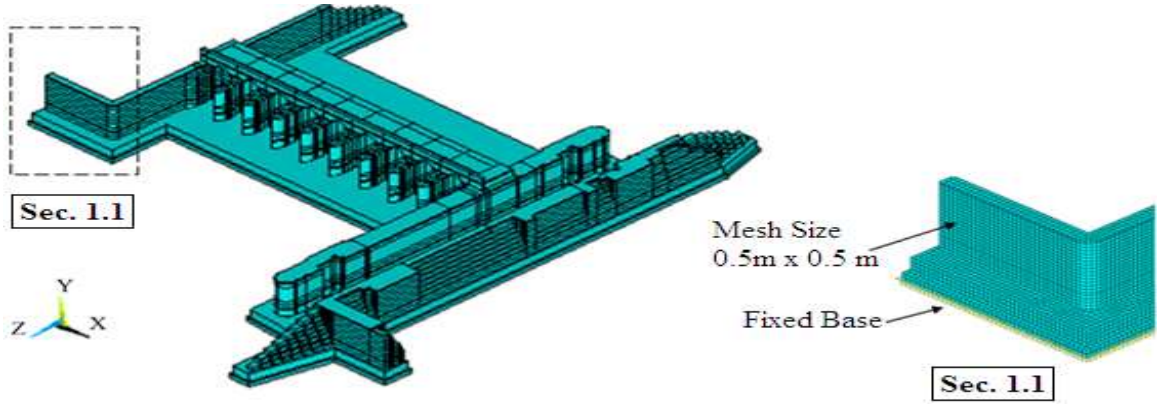

Fig. 10 Initial Model (IM) of the barrage using Solid65 element

Dynamic water masses (M_o&M_1) and spring stiffness (K_1) of the contained water through piers, were calculated according to Housner equations (Housner 1963). These masses were attached to piers or lock using Mass21 element at heights of H_o and H_1, as presented in Table 5. The contained water of pier has the depth at rest (H) of 6.10 m, and half-length of rectangular vent opening (L) = 2.50 m, with width of (B) = 15.50 m (length of pier), and total water mass (M) = 472750 kg. The contained water of lock has the depth of rest (H) of 6.10 m, and half-length of rectangular vent opening (L) equal to 4.0 m, with width of (B) = 79.0 m (length of lock wall), and total water mass (M) of 3855200 kg. To ensure quite accuracy of results, M_o and M_1 were divided into three, and attached on pier every 3.80 m spacing and on lock every 19.75 m in the Z-direction with values of $M_o/6$ and $M_1/3$, respectively. $M_o/6$ masses were directly attached to the wall through its nodes and $M_1/3$ masses were attached to the wall using spring element (Combine14) with stiffness of $K_1/6$, as shown in Fig. 11.

Table 5 Water masses values and heights of assigned locations for pier and lock

	$M_o/6$ (kg)	$M_1/3$ (kg)	H_o (m)	H_1 (m)	$K_1/6$ (kN/m)
Pier	68112	33476	1.80	3.90	102.129
Lock	464419	430542	3.00	2.10	809.235

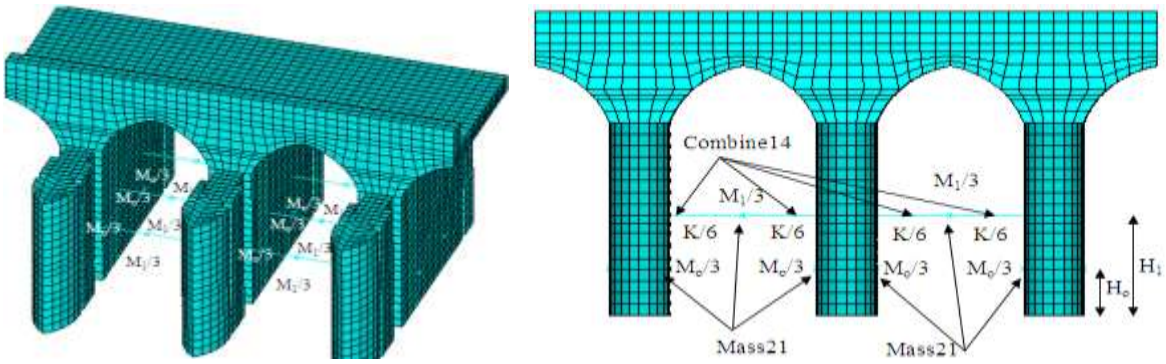

Fig. 11 Attachment of water masses inside the pier

4.4 Updated models (UMs)

Four updated models were conducted to achieve more matching results to the Experimental Work (EW). The characteristics of the updated numerical models (materials, geometry, mesh size, etc.) were unchanged with respect to the initial model. These models were based on updating the Initial Model (IM) by considering the Soil Structure Interaction in the simulation using soil subgrade reactions at each node of the base in the three directions: x, y, and z. The properties of the soil underneath and surrounding the barrage, that were determined from bore holes testing extracted from the site, are presented in Table 6. The structure is settled at foundation level (7.50) on Silty sand layer with a bearing capacity (B_c) equal to 340 kN/m^2 that leads to modulus of subgrade reaction (Ks) of 35000 kN/m` according to Bowles (1988). The value of vertical subgrade reaction (y-direction) was selected as an average value according to Bowles (1988). While, the horizontal subgrade reactions (x, and z-directions) were taken as a ratio of the vertical reaction. This ratio was missing in references and there is not any guide to control it. Even though, the recent studies that were conducted on the estimation of horizontal subgrade reaction were mainly for the pile studies. Therefore, four models were adopted with different ratios of the vertical reaction; 0%, 10%, 30%, and 50%, as tabulated in Table 7. The optimum ratio is the more given matched results with the EW. The surrounding soil (mass and stiffness) was assumed to be neglected to simplify the current investigation. Water effective is also included in these models with same values of IM. Hydrodynamic water pressure was simulated as equivalent mass model.

Table 6 Soil properties

Modulus of elasticity (E_s) (beneath the footing)	1.550 kN/m^2
Modulus of elasticity (E_s) (surrounding the structure)	1.400 kN/m^2
C (cohesion factor)	0.00
ϕ (angle of internal friction)	32°
μ (coefficient of friction)	0.35
γ_s (Unsaturated Soil density)	1.800 kN/m^3
γ_{sat} (Saturated Soil density)	0.800 kN/m^3

Table 7 Soil subgrade reactions

Models	UM1	UM2	UM3	UM4
Horizontal subgrade reaction's ratio (%)	0	10	30	50
Horizontal subgrade reaction (K_x and K_z), in kN/m^3	0	3500	10500	17500

5. Results and discussions

5.1 Water Deformation

The water mode shapes occurred at the lock at 0.3086 Hz and the vents at 0.3931 Hz of the barrage in the FE models. They had the first thirty mode shapes of the results and they occurred at very low fundamental frequencies, as shown in Fig. 12.

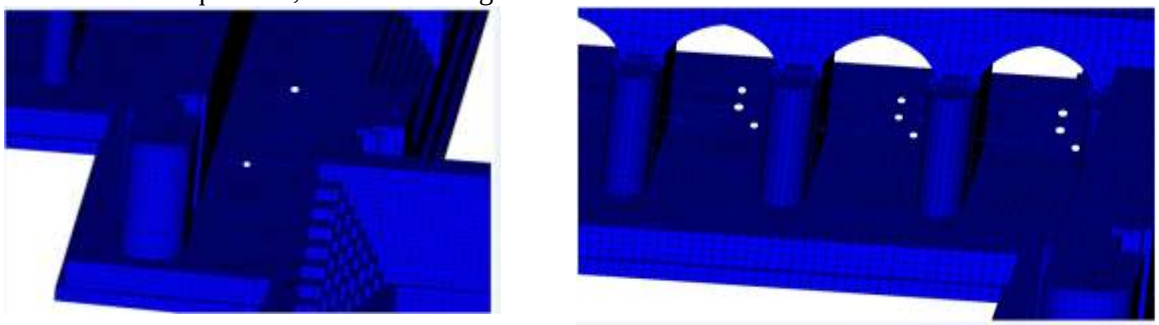

a) Inside the lock (0.3086 Hz) b) Inside the vents (0.3931 Hz).

Fig. 12 The captured water deformations

5.2 Comparison between EW and IM Results

This comparison between the experimental results and the FE results (IM) was conducted to ensure the reality of the obtained results from the IM to match the experimental test as the experimental tests lead to realistic behavior of the tested structure. Therefore, selecting the matching mode shapes with the same deformed shape (as shown in the following figures) of the EW and IM, then comparing the values of its corresponding frequencies together. This comparison showed out a significant variation in results between the EW and the IM, as shown in Fig. 13.

The first mode shape occurred in the EW at a frequency of 7.96 Hz and the IM first mode shape was at 13.18 Hz. They both had the same deformed shape, as a lateral deformed shape of the structural elements, as shown in Fig. 14. Comparing the value of the frequency of the first mode shape for the EW, and IM, it is pointed out that there was a significant difference in the frequencies with a variation of 65.62 % with respect to EW value.

The second mode shape was captured at a frequency of 13.2 Hz in the EW, while the IM results presented the same deformation of the tested vent at 20.16 Hz. This mode shape was similar to the first one with a lateral deformation, but without a symmetrical deformation of the two piers. One pier deformed with larger displacement than the other. The relative movement of the two piers indicates that one deformed while the other did not deform, as illustrated in Fig. 15. The difference in the value of the corresponding frequencies was equal to 52.75% with respect to EW value that was less than the

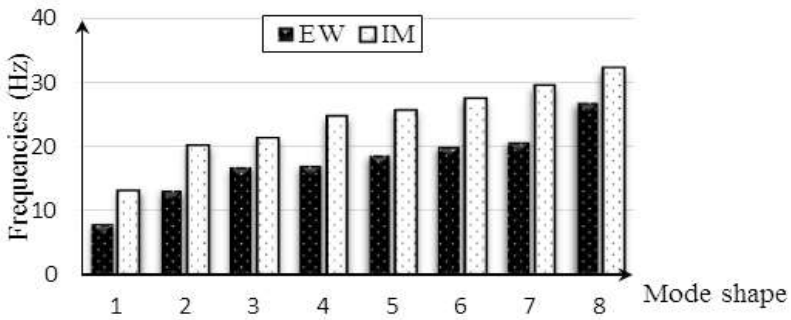

Fig. 13 Comparison of results between EW and IM

first mode shape.

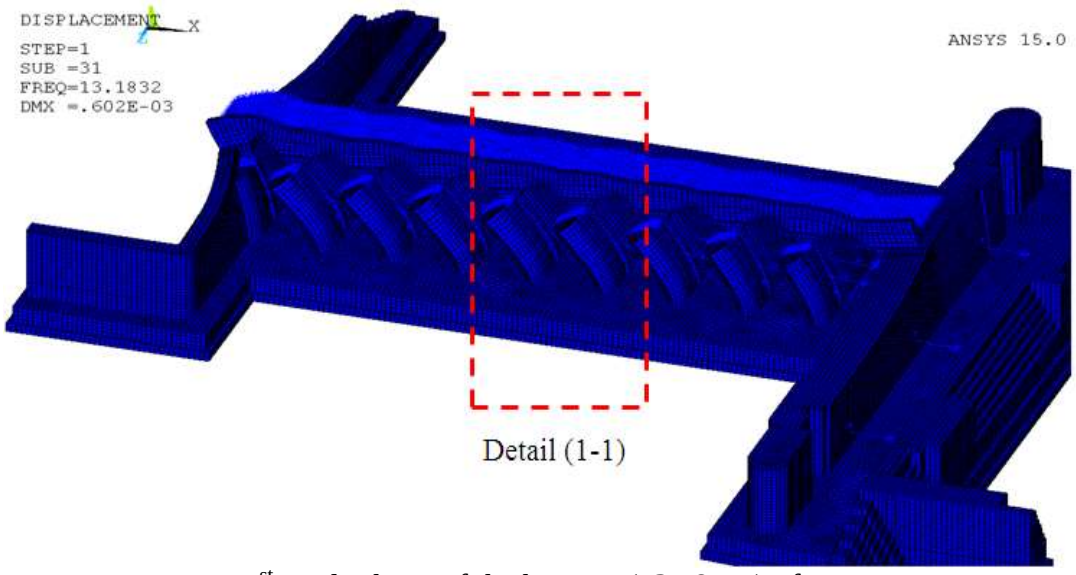

1st mode shape of the barrage (13.18 Hz) of IM

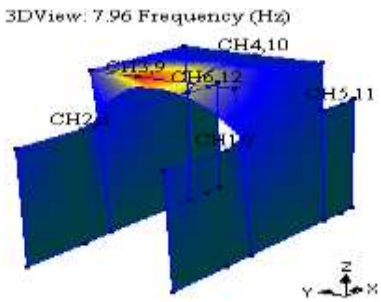

1st mode shape at 7.96 Hz of EW

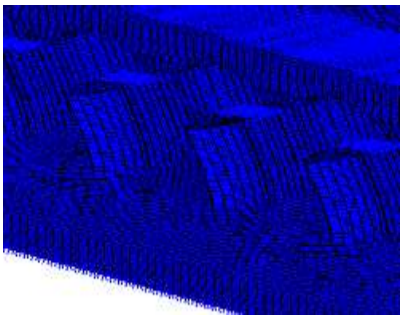

Detail (1-1) in IM at 13.18 Hz

Fig. 14 First mode shape of EW and IM

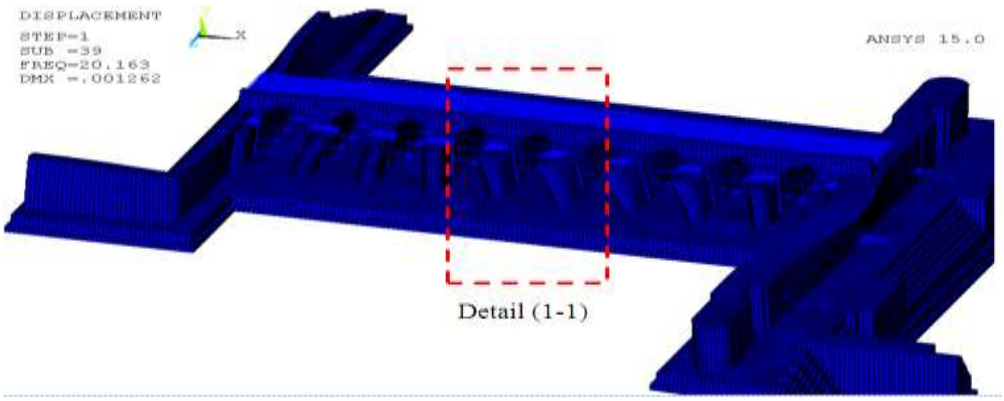

2nd mode shape of the barrage (20.16 Hz) of IM

Fig. 15 Comparison of the second mode shape between EW and IM, continue

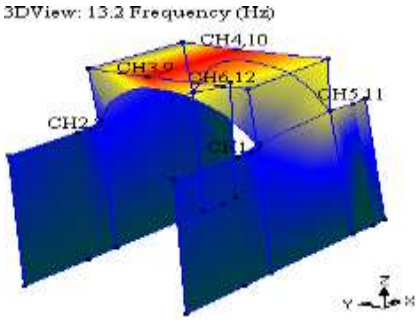

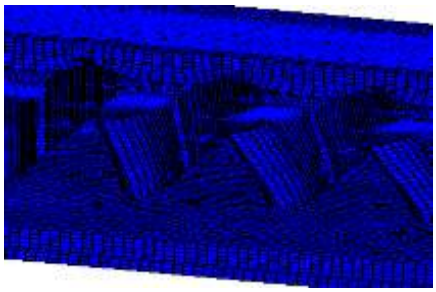

2nd mode shape at 13.2 Hz of EW Detail (1-1) in IM at 20.16 Hz

Fig. 15 Comparison of the second mode shape between EW and IM

In the comparison between the frequency value of the third mode shape for the EW, and the IM, a difference was noticed with 27.38 % with respect to the EW. The EW showed this mode shape at 16.8 Hz and the IM was at 21.40 Hz. This mode shape had a different deformation than the first and second mode shapes. Obviously, the movement of the arch and the road of the barrage was in the opposite direction of the piers' one, as represented in Fig. 16. These movements were captured the same in both EW and IM with different values of frequency. Another mode shape was captured at 17.0 Hz form the EW, and at 24.71 Hz from the IM. This mode shape has an upward and downward (vertical) movement of the piers (see Fig. 17), that was different with the third mode shape. The lateral deformations of the piers and the opposite deformations of the arch, and the road were still the same as the third mode shape. This vertical movement occurred clearly at CH1, CH2, CH5, and CH6 (vertical recording channels) in the EW. The fifth mode shape occurred with a frequency of 18.6 Hz in the EW, and with a frequency of 25.67 Hz in the IM. The difference in the corresponding values of frequency was 38.03 Hz in percent with respect to EW. The deformed shape of the piers, arch, and the road had a quite matching deformation with the third mode shape, the change was in the deformation of the road and the arch. There was a significant relative deformation between the upstream and downstream edges of the road (vertical deformation occurs) that is similar to a torsion deformation, as shown in Fig. 18. The deformation of the second mode shape took place again at the sixth mode shape of the barrage, but with a vertical deformation (upward and downward) of the center of the arch at the upstream, as illustrated in Fig. 19. It was captured in the EW, and IM at 20.1 Hz, and 27.43 Hz, respectively. There was also a significant difference in the values of the frequency with a percent of 36.46 with respect to EW.

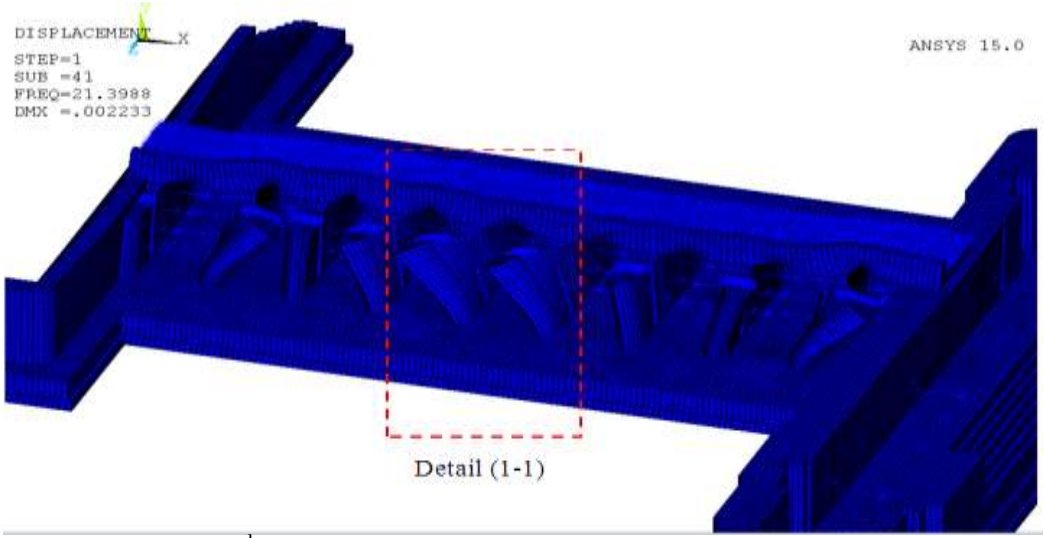

3rd mode shape of the barrage (21.40 Hz) of IM

Fig. 16 The deformed shape of the third mode of EM and IM, continue

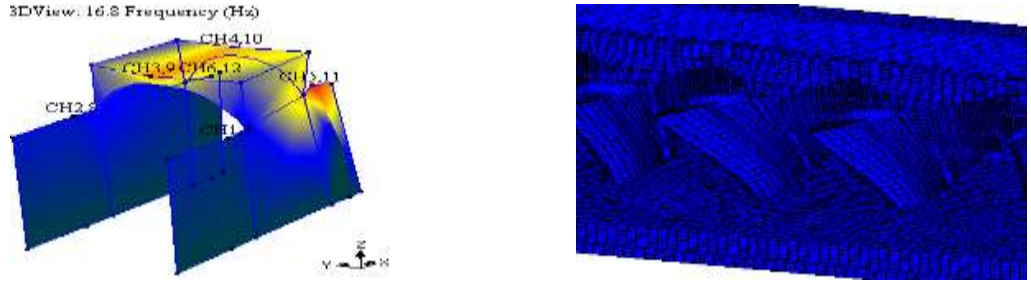

3rd mode shape at 16.8 Hz of EW Detail (1-1) in IM at 21.40 Hz

Fig. 16 The deformed shape of the third mode of EM and IM

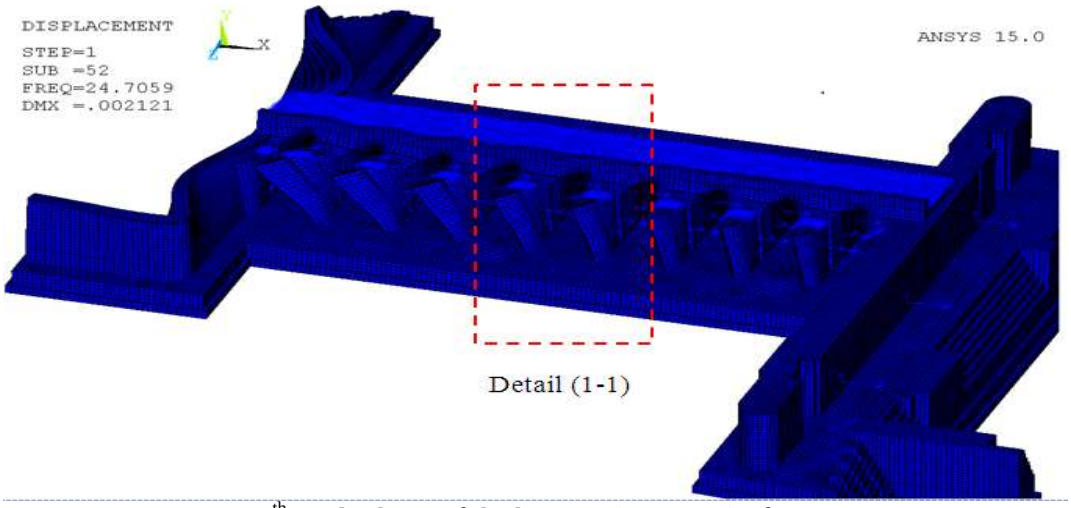

4th mode shape of the barrage (24.70 Hz) of IM

Fig. 17 Comparison between the EW and IM for the fourth mode shape, continue

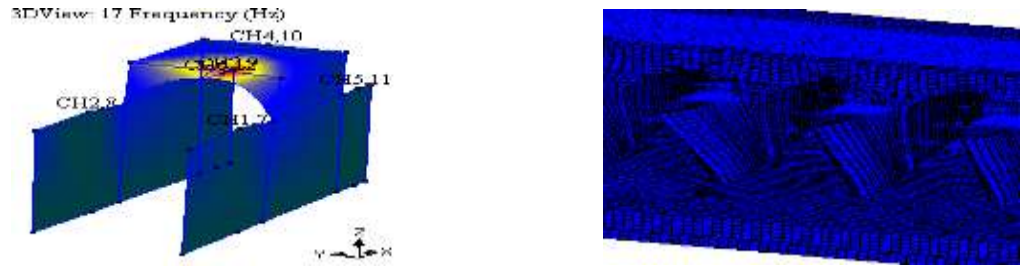

4th mode shape at 17.0 Hz of EW Detail (1-1) in IM at 24.70 Hz

Fig. 17 Comparison between the EW and IM for the fourth mode shape

Investigating the seventh mode shape of the barrage was at a near frequency to the sixth one where it was 20.8 Hz and 29.50 Hz of EW and IM results, respectively. In this current mode shape (see Fig. 20), all structural elements of the tested vent deformed vertically with small lateral deformation, that was noticed in both EW, and IM results. Huge deformation of the whole barrage including the tested vent was observed in the 8th mode shape. This deformation caused mainly due to the occurrence of the vertical and lateral movements together with huge deformation, as shown in Fig. 21. It could be considered as a complex mode shape. This mode shape was recorded in the EW at a frequency of 26.9 Hz. It is found at 32.11 Hz in the IM. According to these frequencies of the 8th mode shape that were captured in the EW, and IM, the difference was 19.36 % with respect to EW. The different percentages of the frequencies' value between the EW, and IM were estimated for the eight mode shapes. They all had a great different percentage value; the maximum was 65.62 %, and the minimum was 19.36 % as mentioned before. Some parameters may be the source of the difference: considering the fixed base condition, differential cracking/stiffness of the structure, considering Houssner model, accuracy of mass between FE model and the real model, and the lateral boundary conditions. Thus, minimize these differences is a major issue that has to be solved and correlated. The proposed step has

to update the finite element model (IM) to match closely as possible as the EW results. The method of correlation was based on replacing the fixed boundary condition of the base with the subgrade reactions under the base of the barrage that was called Updated Models (UMs).

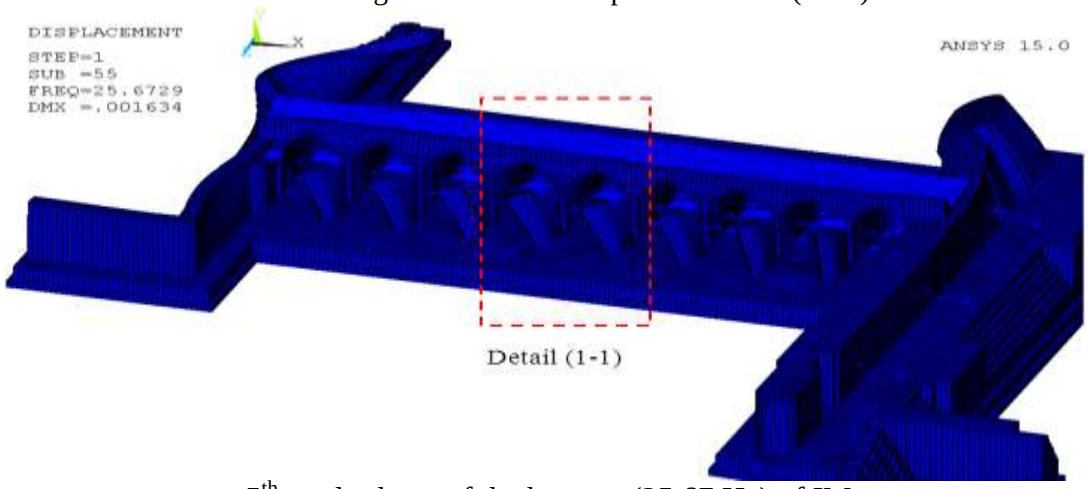

5th mode shape of the barrage (25.67 Hz) of IM

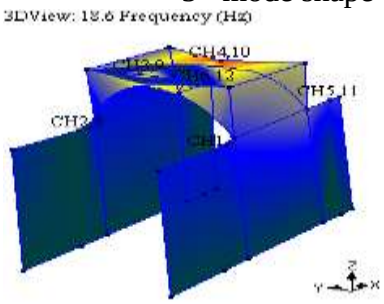

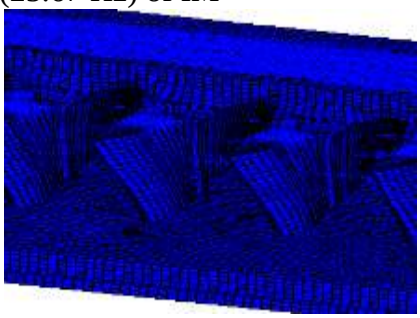

5th mode shape at 18.6 Hz of EW Detail (1-1) in IM at 25.67 Hz

Fig. 18: The fifth mode shape of EW and IM

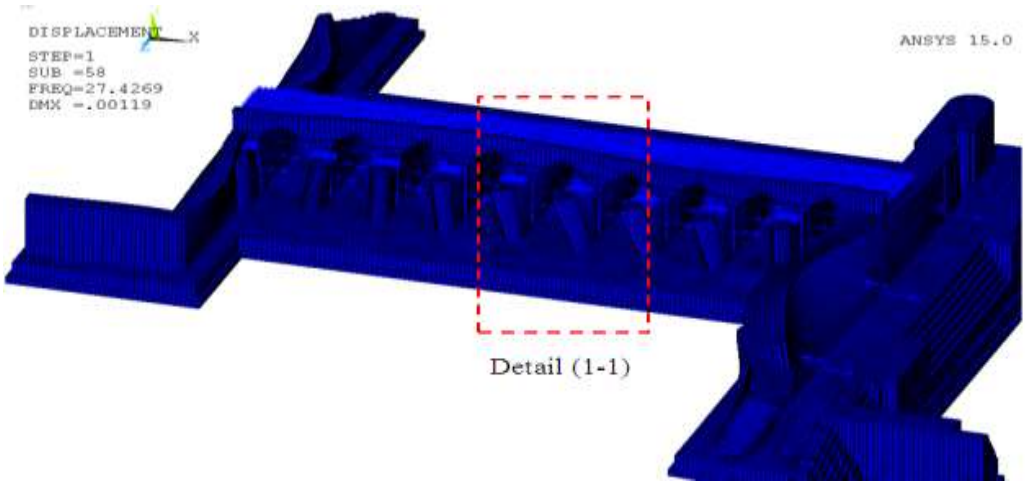

6th mode shape of the barrage (27.43 Hz) of IM

Fig. 19 The sixth deformed shape of EW and IM, continue

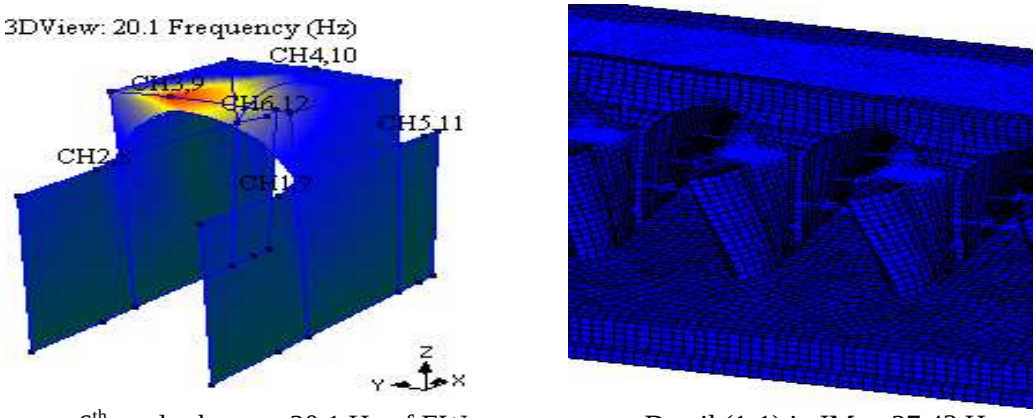

6th mode shape at 20.1 Hz of EW Detail (1-1) in IM at 27.43 Hz

Fig. 19 The sixth deformed shape of EW and IM

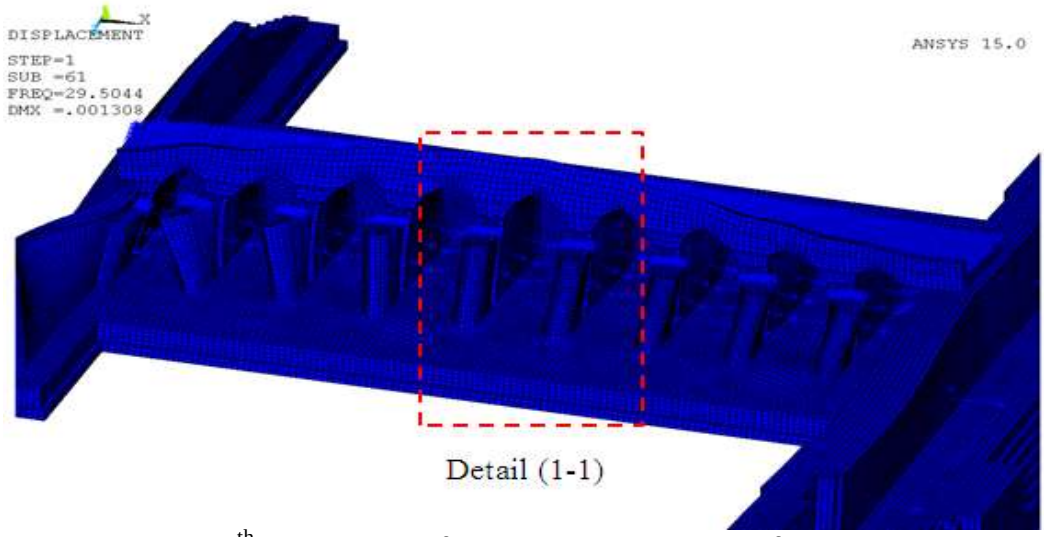

7th mode shape of the barrage (29.50 Hz) of IM

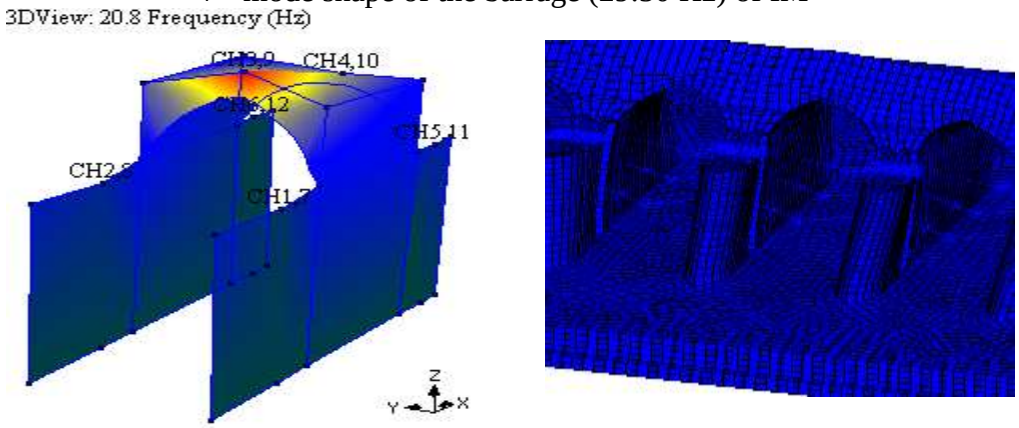

7th mode shape at 20.8 Hz of EW Detail (1-1) in IM at 29.50 Hz

Fig. 20 The seventh deformed shape of EW and IM

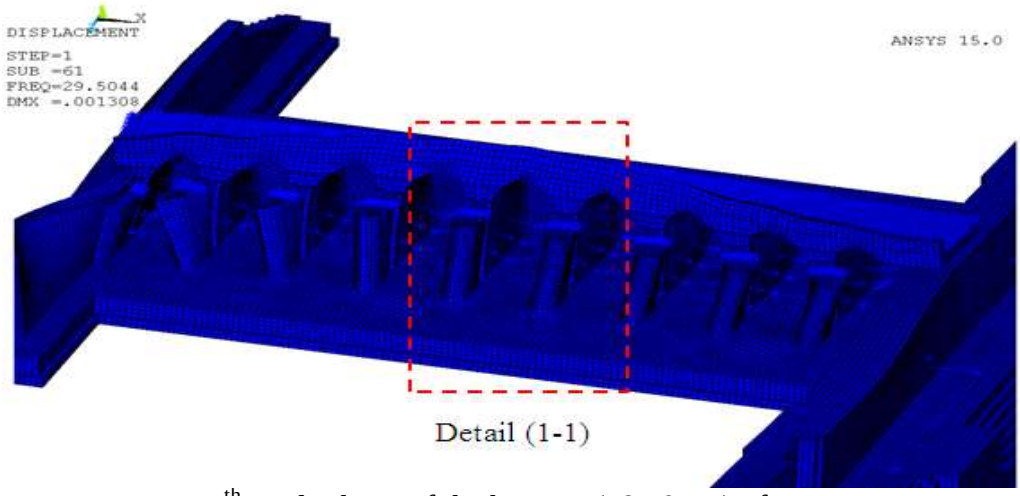

7th mode shape of the barrage (29.50 Hz) of IM

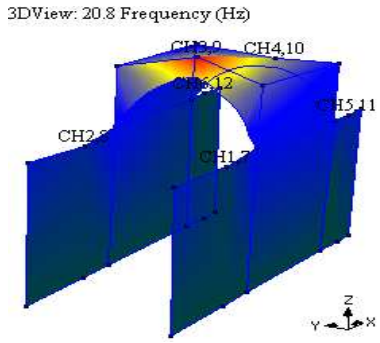

7th mode shape at 20.8 Hz of EW

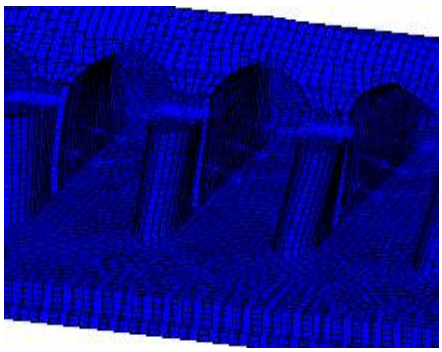

Detail (1-1) in IM at 29.50 Hz

Fig. 20 The seventh deformed shape of EW and IM

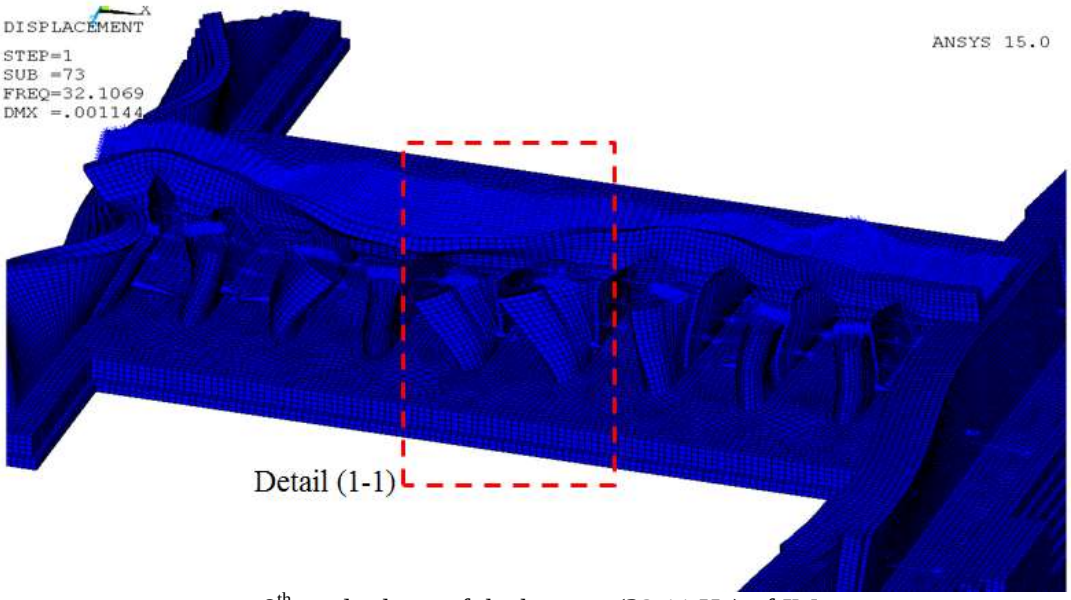

8th mode shape of the barrage (32.11 Hz) of IM

Fig. 21 The occurred distortion in the 8th mode shape of EW and IM, continue

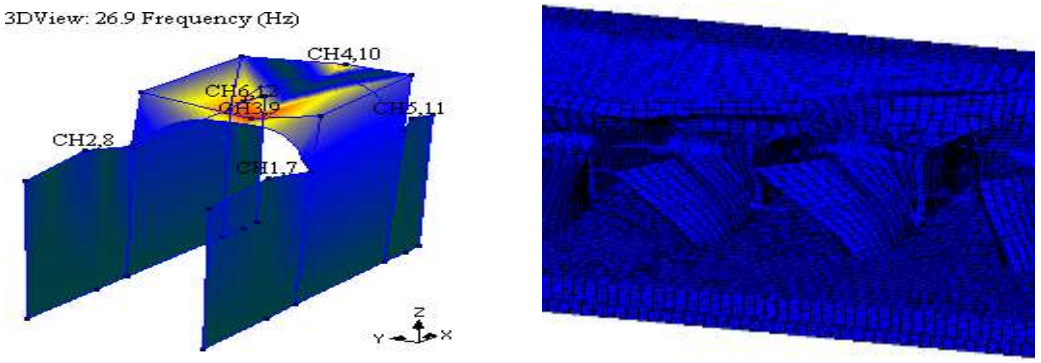

8th mode shape at 26.9 Hz of EW Detail (1-1) in IM at 32.11 Hz

Fig. 21 The occurred distortion in the 8th mode shape of EW and IM

5.3. Results of UM1 and UM2

The first two mode shapes of UM1 and UM2 that considered the horizontal subgrade reaction with a ratio equal to 0% and 10% from the vertical subgrade reactions respectively are presented in Fig. 22 to Fig. 25. From these figures, it can be noticed that these ratios make the barrage deforming as a rigid body movement. Lateral, rotation and torsional movement of the overall structure occurs due to the less resistance of the horizontal subgrade reactions. The 0% and 10% are not enough to let the structural elements deform, as the base boundary condition acts like a roller support. Besides that, the values of frequencies are significantly out of range in comparing with the EW. The comparison between the results of the two models (UM1 and UM2) and the EW results is impossible as there are no any matching mode shapes.

5.4. Comparison between EW and UM3

The comparison between the experimental work (EW) and the numerical (UM3) is presented and showed in the current section. This model gives the matching mode shapes in shape with IM and EW as shown in Fig. 26 for the first mode shape as example. The difference between the UM3 results decreased to be ranged from 4.75% to 0.16% with respect to the EW results, as tabulated in Table 8. The description of the eight mode shapes of UM3 are the same as mentioned in the EW-IM comparison. The same deformations of structural elements have occurred in each mode shape. The SSI causes some flexible deformations in the structure and its base and that were observed in the UM3 mode shapes. In Fig. 26, the first mode shape of UM3 was observed at 7.99 Hz. This value was almost the same value of EW (7.96 Hz). The difference percentage is decreased to a very small value: 0.36% with respect to EW value. The second mode shape was captured at a frequency of 13.83 Hz in the UM3. This mode shape was also similar to the 2nd mode shape of EW. The difference in the value of the corresponding frequencies was equal to 4.75% with respect to EW value. This value is the maximum difference between the EW and UM3 results that was observed through the eight mode shapes. In the comparison between the frequency value of the third mode shape for the EW and the UM3, a difference was noticed with 0.16% with respect to the EW. The EW showed this mode shape at 16.8 Hz and the UM3 was at 16.83 Hz.

The fourth mode shape was clearly noticed at 16.94 Hz for the UM3. This mode shape has a downward and upward vertical movement of the piers. The difference between the EW and the UM3 is also small for this mode shape. There is just 0.38 difference percentage with respect to the EW. Another mode shape was obtained at 18.21 Hz in UM3 (5th mode shape). The difference was 2.08% with respect to EW. This mode shape has a significant torsional deformation in the road of the barrage. Also, the lateral deformation of the pier was noticed. The second mode shape was obviously noticed again at the sixth mode shape of the barrage at a frequency of 20.17 Hz (from UM3), with the addition of the vertical deformation of the arch and the road. The value of the frequency of UM3 increases with a percent of 0.34 with respect to EW. The seventh mode shape occurs at 20.21 Hz for UM3 and it occurs with a frequency of 20.8 Hz for EW. In this model, the vertical deformations of all structural elements were noticed with small lateral deformations. In this model, the difference

between the frequencies as obtained from EW and UM3 is 2.83% with respect to EW results. The deformation of the whole barrage occurred at 26.51 Hz (the 8th mode shape). This mode shape was recorded in the EW at a frequency of 26.9 Hz. The difference is 1.47% with respect to the EW.

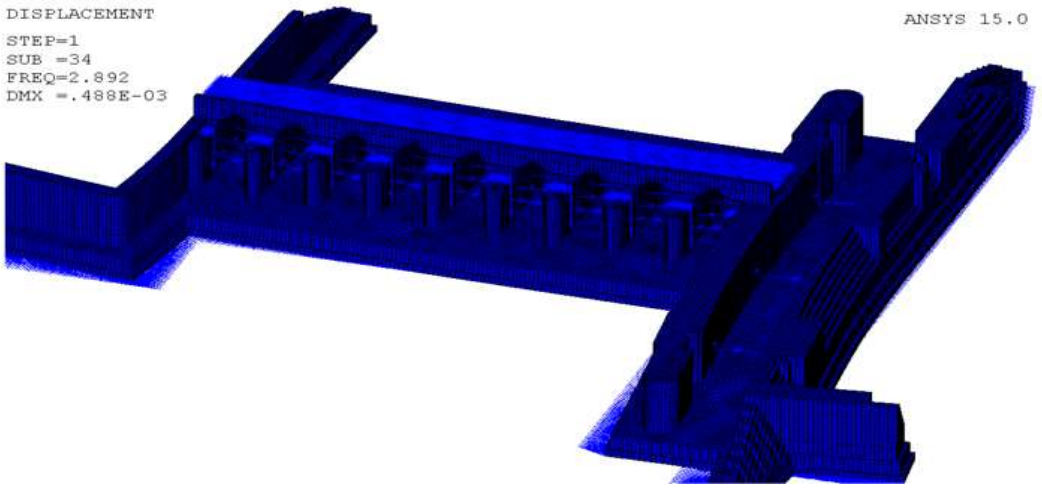

Fig. 22 1st mode shape of UM1 (2.892 Hz)

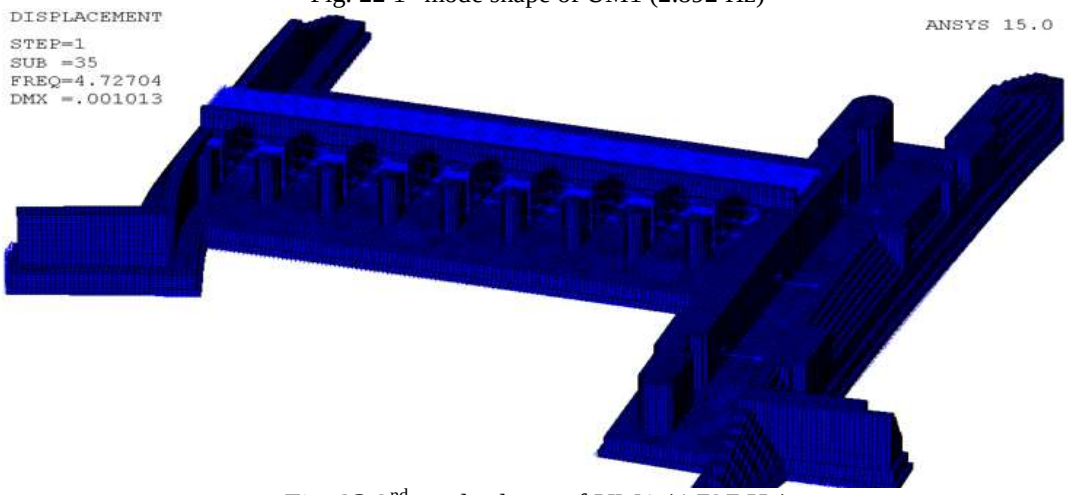

Fig. 23 2nd mode shape of UM1 (4.727 Hz)

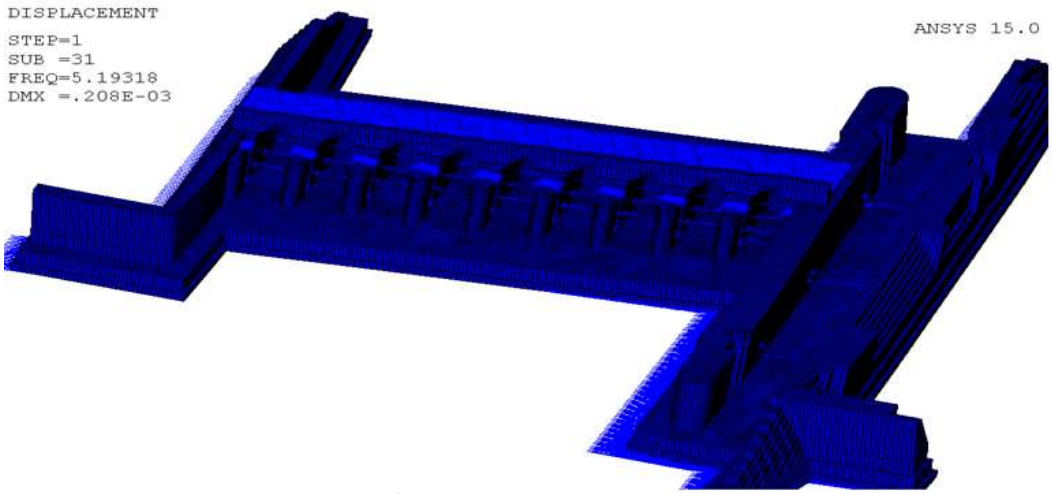

Fig. 24 1st mode shape of UM2 (5.193 Hz)

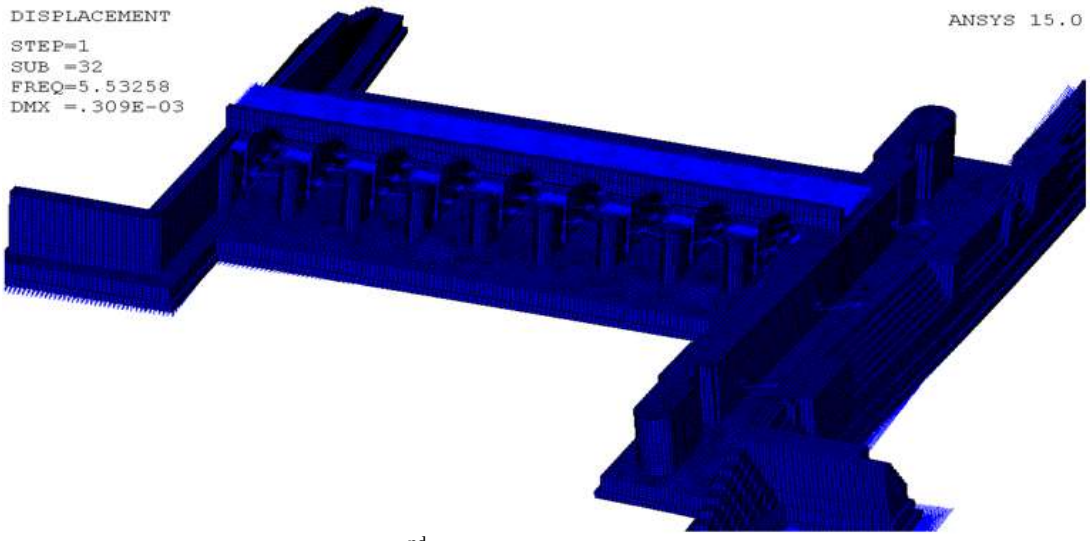

Fig. 25 2nd mode shape of UM2 (5.532 Hz)

5.5 Comparison between EM and UM4

This comparison shows an increment again in the difference percentage between the EW and UM4 results as concluded in Table 9. The first mode shape was captured at 9.15 Hz of the UM4. This is more than the EW with a percentage of 14.95 with respect to EW. The 2nd mode shape was recorded at a frequency of 14.18 Hz (UM4). 10.33 percentage differences were observed between the EW and UM4's value of the frequency of the third mode shape. The fourth mode shape occurred with a value of frequency that is more than the EW with 13.89%. The EW's mode shape was at 17.0 Hz, and the UM4's mode shape was at 19.36 Hz. Capturing the 5th mode shape was at a frequency of 20.47 Hz. It has with 10.04% a difference in the value of frequency than the EW with respect to the EW. The difference percentages between the EW, and the UM4 for the 6th, 7th, and 8th mode shape were 7.19%, 4.14%, and 1.46%, respectively. These mode shapes have the same deformation with a change in the value of frequency than the EW, IM and UM3 as represented in Fig. 27: for the first mode shape as example.

5.6 Soil-structure interaction effect

After analyzing the data recorded from the field testing, it was compared with the IM results. This comparison showed a significant difference in the value of frequencies between the EW and the IM (see Fig. 28). Those differences were supposed to be there, as the IM considered the fixed base condition. This condition increased the value of frequencies due to the large stiffness of the base/structure. The updating technique was based on adopting the SSI into the FE model. Therefore, soil subgrade reactions (K_s) were applied under the base of the barrage in the three directions; x, y, and z-directions. An average value of the Bowles' subgrade reaction (Bowles 1988) was used for the vertical springs (K_y) according to the soil properties under the studied barrage. The horizontal subgrade reaction under the raft (K_x, and K_z) was adopted with various ratio of the vertical one; 0%, 10%, 30%, and 50% (the four Updated Models: UM1, 2, 3, and 4) to get closely matched results to the EW. The horizontal subgrade with 0% and 10% of the vertical reaction are not enough to let the structural elements deform, as the base boundary condition acts like a roller support (as presented in section 3.1) so UM3 and UM4 models only were compared with the IM and EW results for estimating the optimum ratio of horizontal subgrade reaction. It was clearly observed that the UM3 with the ratio of 30% of the vertical subgrade reaction gives more matching results to the EW with differences ranged from 0.16% to 4.75% with respect to the EW.

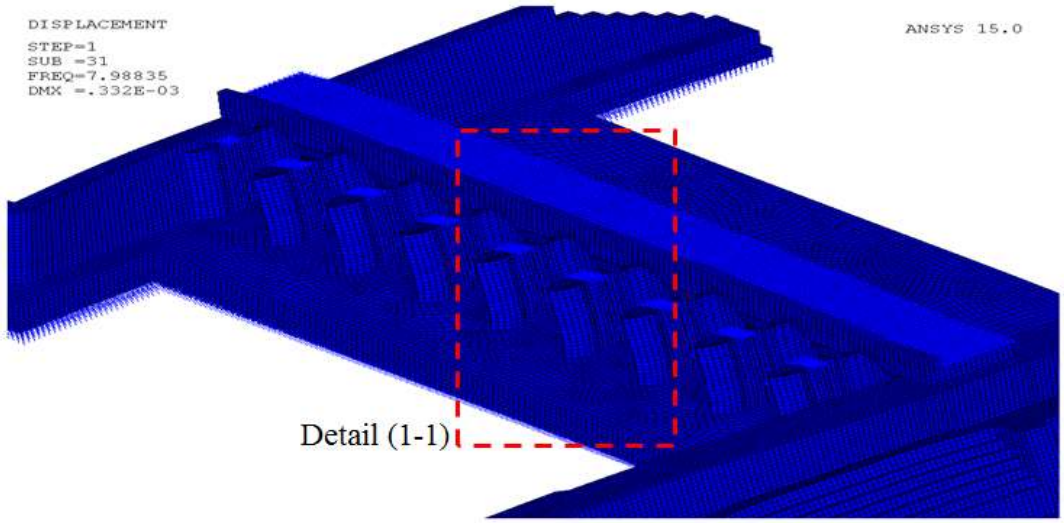

1st mode shape of the barrage (7.99 Hz) of UM3

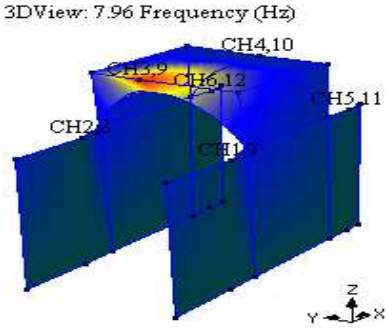

1st mode shape at 7.96 Hz of EW

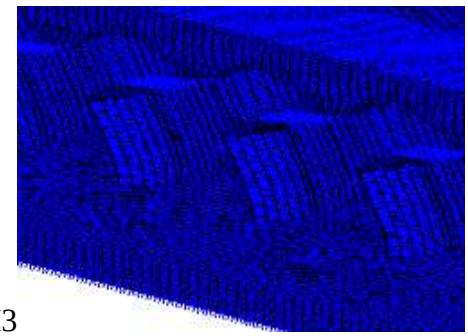

UM3

Detail (1-1) in UM3 at 7.99 Hz

Fig. 26 The first mode shape of UM3 and EW

Table 8 EW and UM3 results

Mode shape		1st	2nd	3rd	4th	5th	6th	7th	8th
Frequency (Hz)	EW	7.96	13.2	16.8	17.0	18.6	20.1	20.8	26.9
	UM3	7.99	13.83	16.83	16.94	18.21	20.17	20.21	26.51
Difference (%)		0.36	4.75	0.16	0.38	2.08	0.34	2.83	1.47

Table 9 Comparison between experimental (EW) and numerical results (UM4)

Mode shape		1st	2nd	3rd	4th	5th	6th	7th	8th
Frequency (Hz)	EW	7.96	13.2	16.8	17.0	18.6	20.1	20.8	26.9
	UM4	9.15	14.18	18.53	19.36	20.47	21.54	21.66	27.29
Difference (%)		14.95	7.43	10.33	13.89	10.04	7.19	4.14	1.46

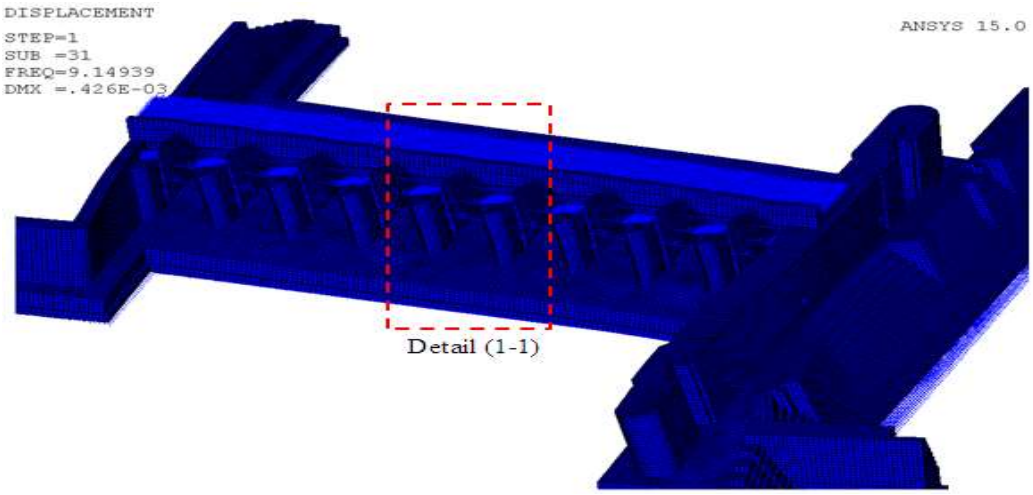

1st mode shape of the barrage (9.15 Hz) of UM4

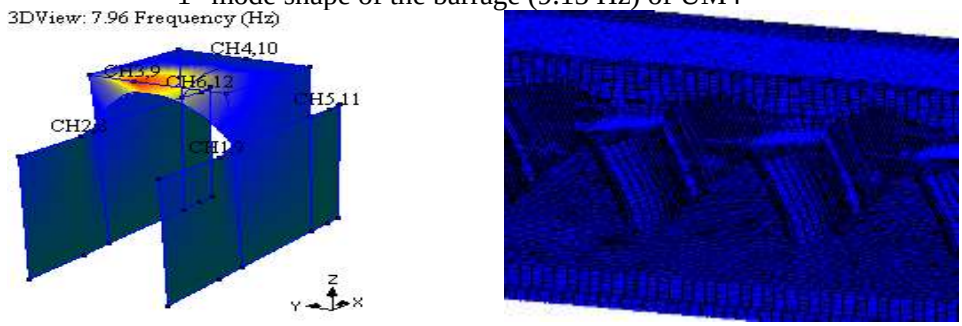

1st mode shape at 7.96 Hz of EW Detail (1-1) in UM4 at 9.15 Hz

Fig. 27 The first mode shape of EW and UM4

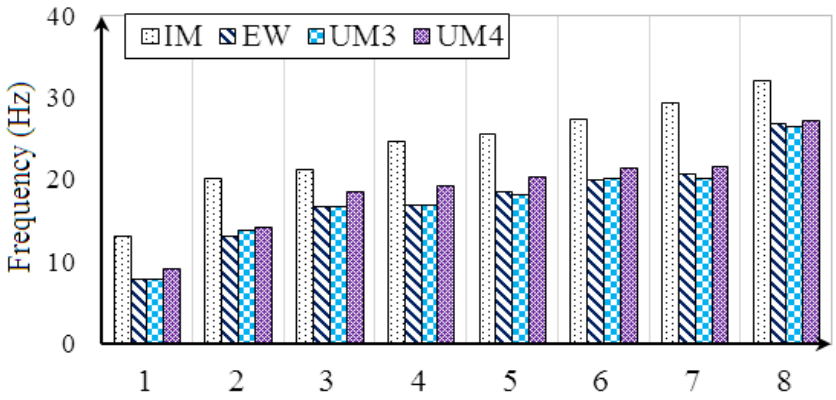

Fig. 28 The frequencies of the IM, EW, UM3, and UM4

6. Conclusions

The current study was adopted to investigate the dynamic properties of the Old Rayah Menoufia Barrage – Egypt in terms of mode shapes, natural frequencies, and damping ratio. This barrage is an oldest existing structure in Egypt that was permitted to be tested by the Construction Research Institute (CRI) - National Water Research Center (NWRC) - Egypt. Through this investigation, numerical and experimental modal analyses are involved. The numerical analysis included Initial Model (IM) and four Updated Models (UM1, 2, 3, and 4). The IM was not considered Soil-Structure Interaction (SSI). In the UMs, soil subgrade reactions (K_s) were applied under the base of the barrage in the three directions; x, y, and z-directions. The horizontal subgrade reactions under the raft (K_x, and K_z) were adopted with various ratio of the vertical one; 0%, 10%, 30%, and 50% to get closely matched results to the EW. The conclusions of the current research are written below:-

- For testing these types of structure, there is a major need for a pre-finite element model to predict the results of the Experimental Work (EW) and control the factors that affect the accuracy of the results.

- For more accurate results of the EW, large numbers of sensors are required to capture all responses of each structural element of the barrage.
- With adequate numbers of sensors, the location of the sensors plays a potential role to capture the predicted response that matches the FE model.
- When the structure consists of typical replicated vents, choosing an intermediate vent to be tested, can give an adequate realistic indication of the structure's behavior.
- The initial model gave higher values of the natural frequencies than the experimental results.
- The ratio percentages of the horizontal subgrade reactions with value of 0% and 10% from the vertical reactions cause an overall shear movement of the structure with too small value of natural frequencies. The results of these models (UM1 and UM2) are significantly far away in either the mode shapes or the value of the natural frequencies.
- Considering the horizontal subgrade reactions with the ratio of 30% of the vertical subgrade reaction gives more realistic results with more closely matched mode shapes and natural frequencies to the EW. The difference between the results of the EW and the UM3 is so small.
- The ratio of 50% (UM4) caused an increase in the stiffness of the structure that is noticed in the increase of frequencies' value.

7. Further Works

More studies are still remained to be investigated for this type of structure. The listed below are the future works that are supposed to nearly studied to improves the analysis:

- Capturing the full response of all structural elements of the barrage using sufficient numbers of sensors/instruments, and studying the difference when testing a typical replicated vent.
- Carrying out the three-dimensional (3D) modeling of water using acoustic elements, to investigate its effect on results comparing with Housner simulation.
- Performing a study to discover the effect of the surrounding soil beside the abutments with considering the water table and the real profile of the soil on the results.
- Employing 3D model to simulate the soil and investigate the required depth, and width of soil that should be considered through the analysis, and compare it with the subgrad reactions method of Bowles.

References

Kortiš J., Daniel L., Škarupa M. and Ďuratný M., (2016) "Experimental modal test of the laboratory model of steel truss structure," *Civil and Enviro. Eng*., **12**(2), 116-121.

Shaheen Y. Eltaly, B.and Kameel, M. (2013) "Damage detection of ferrocement tanks using experimental modal analysis and finite element analysis," *Con. Research Letter*, **4**(2), 598-608.

Rahman A., (2009) "Final research report theoretical model for damage and vibration response in concrete bridges," Technical Report, Research Management Centre (RMC), UniversitiTeknologi Malaysia

Payab M. and Ahmadifar F., (2015) "A Comparative review on operational modal analysis methods," *Cumhuriyet Unive. Faculty of Science: Science J. (CSJ)*, **36**(3), Special Issue, 3302-3311.

Brownjohn J. (2003) "Ambient vibration studies for system identification of tall buildings," *Earthquake Eng. & Struct. Dynamics*, 32, 71-95.

Diaferio M., Foti D., Gentile C., Giannoccaro NI, Saisi A (2015) "Dynamic testing of a historical slender building using accelerometers and radar," 6th International Operational Modal Analysis Conference, IOMAC 2015.

Comanducci G., Cavalagli N., Gioffré M., Trequattrini M. and Ubertini F., (2017) "Ambient vibration testing of a monumental fountain by contact and non-contact sensing techniques," Procedia Eng., **199**, 3338–3343.

Bajric A., Brincker, R. and Thöns S. (2015) "Evaluation of damping estimates in the presence of closely spaced modes using operational modal analysis techniques," In Proceedings of the 6th International Operational Modal Analysis Conference, IOMAC 2015, Denmark.

Balmes E., Chapelier C., Lubrina P., and Fargette P., (1995) "An evaluation of modal testing results based on the force appropriation method," Interernational Modal Analysis Conference, United States**, 1**(1), 47–53.

Khalil A., Greimann L., Wipf T., and Wood D., (1998) "Modal testing for nondestructive evaluation of bridges" 1998 Transportation Conference Proceedings, Antwerp, Belgium, **3**, 109–112.

Pandey D., Bhargava A., Chakrabortty P., Gupta, P., and Jain, C., (2004) "Dynamic characteristics of a barrage at various stages of construction," 13th World Conference on Earthquake Engineering, Canada, 1778, 5–10.

Garaygordóbil A., (2005) "Dynamic identification and model updating of historical buildings. State-of-the-art review," *Struct. Analysis of Historical Constr.*, 1988, 499–504.

Ramos F., Roeck G., Lourenço B., and Campos-Costa A., (2006) "Vibration based damage identification of masonry structures," *Struct. Analysis of Historical Constr.*, 1 (1996) 641–650.

Haritos N., Khalaf H., and Chalko T., (1995) "Modal testing of a skew reinforced concrete bridge," *Immunization Advisory Centre*, IMAC, 703–709.

Eltaly B., Saudi G., Ali R., and Kandil, K., (2014) "Experimental and FE modal analysis for elevated steel water tanks," *Inter. J. Eng. Research & Technology (IJERT)*, **3**(1), 213–222.

Calcina V., Eltrudis L., Piroddi L., and Ranieri G., (2014) "Ambient vibration tests of an arch dam with different reservoir water levels: Experimental results and comparison with element modelling," *The Scientific World J., Hindawi Publish. Corpor.*, **2014**, 1–12.

Kandil K., Saudi G., Eltaly B., & Abo El-khier M., (2016) "Seismic response of a full-scale wind turbine tower using experimental and numerical modal analysis," *Inter. J. Advanced Struc. Eng.*, **8**(4), 337–349.

Saudi G., Eltaly B. and El-khier M., (2016) "Dynamic behavior of A full-scale wind turbine tower under seismic loading," *Inter. J. Civil Struc. Eng.*, **3**(3), 98–104.

Housner G., (1963) "*The dynamic behavior of water tanks," Bullet. Seismolog*. Society of America., **53**(2), 381–387.

Charatpangoon B., Kiyono J., Furukawa A., and Hansapinyo C., (2014) "Dynamic analysis of earth dam damaged by the 2011 off the pacific coast of tohoku earthquake," *Soil Dyna. Earth. Eng*., **64**, 50–62.

Livaoğlu R. and Doğangün A., (2006) "Simplified seismic analysis procedures for elevated tanks considering fluid-structure-soil Interaction," *J. Fluids Struc*., **22**(3), 421–439.

Axisa F. and Antunes J., (2007) "Modeling of mechanical system: fluid structure interaction," Handbook.

Kuo H., (1982) "Fluid–structure interactions: Added mass computations for incompressible fluid," Technical Report.

Li P., Lu X., Chen B., and Chen Y., (2004) "Computer simulation on dynamic soil-structure interaction System," 13th World Conference on Earthquake Engineering, Canada, 3233, 1–15.

Raychowdhury P., and Singh P., (2012) "Effect of nonlinear soil-structure interaction on seismic response of low-rise SMRF buildings," *Earth. Eng. and Eng. Vib.*, **11**(4), 541-551.

Swapnal P., (2015) "Effect of soil structure interaction on gravity dam," *Inter. J. Science, Eng. and Technology Research (IJSETR)*, **4**(4), 1046–1053.

Varughese A. and Nikithan S., (2016) "Seismic behavior of concrete gravity dams," *Advances in Comput. Design*, **1**(2), 195–206.

Valeti B., Ray-Chaudhuri S., and Raychowdhury P., (2016) "Seismic response of an elevated aqueduct considering hydrodynamic and soil-structure interactions," *Inter. J. Advanced Struc. Eng.*, **8**, 53–71

Farghaly A., (2017) "Seismic analysis of adjacent buildings subjected to double pounding considering soil–structure interaction," *Inter. J. Advanced Struc. Eng.*, **9**, 51–62, 2017.

Bowles J. (1988) "Foundation analysis and design," McGraw-Hill Publishing Company, USA.

Sogreah, A., (2005) "Feasibility study for rehabitation / reconstruction of Zefta barrage phase 2- data collected and analyisis of options," Technical Report, Egypt.

Ace A., (1996) "Geotechnical investigation for Zefta barrage and reactivation of old piezometers," Factual Report, Egypt.

Lahmeyer, A., (2004) "Small hydro power installations on the delta barrages / Egypt pre-tender design investigations, " Technical Report, Vol. 1.

Mohamed A., (2015) "Structural damage detection of slabs using limited measurements," Ph.D. Thesis, Zagazig University, Egypt.

ANSYS (2013) "ANSYS mechanical user's guide," pp. 1858.

Eltaly B., Bembawy A., Meleka N., and Kandil K., (2017) "Structural behavior of recycled aggregates concrete filled steel tubular columns," *Challenge J. Con. Res. Letters*, **8**(1), 17–28.